# MASTERING THE CRYOGENIC FRONTIER: PREDICTING SLOSHING IN CRYOGENIC PROPELLANT TANKS

**Daniel Hauser,[*] Mohammad Kassemi,[†] and Olga Kartuzova[‡], Michael Baker[§], John Mishic[**]**

In recent years, NASA has undertaken the development and validation of computation fluid dynamic (CFD) models for predicting cryogenic two-phase sloshing within propellant tanks. These models have been rigorously anchored against cryogenic ground tests that induce sloshing, as well as limited microgravity tests. The primary focus of these models is to accurately predict the two-phase condensation and, at times, evaporation within the cryogenic propellant. This approach is important for estimating the required autogenous and/or helium pressurant for completing propulsion system burns or ensuring adequate pressure for in-space propellant transfers.

Unlike in hypergolic propulsion systems, where the propellant is stored at room temperature, cryogenic propellant is highly volatile. Therefore, ensuring the accurate estimation of pressurant necessitates the precise modeling of two-phase interfacial heat and mass transfer processes. This paper aims to provide an overview of NASA's continuing efforts in developing and validating these CFD models, with particular emphasis on benchmark cases with sloshing that enhances phase change, tracing their historical development, and demonstrating their predictive accuracy when compared to test results.

## INTRODUCTION

Since the 1960s, NASA has been exploring cryogenic propellant technologies for space propulsion, focusing on improving the efficiency of space vehicles[1]. One of the main challenges during these operations is handling volatile cryogenic propellants under low-gravity conditions of space, where the movement of these fluids, known as sloshing, can be more pronounced. When pressurized with autogenous pressurant, the sloshing of the propellant can cause the vapor to condense from the ullage requiring additional pressurant and heating the liquid. These issues make controlling the pressurant used to extract the propellant, either for transfer or for use in engines, more complex.

NASA and its partners have conducted various ground tests to better understand these challenges and the necessary pressurant requirements. Managing the sloshing in propellant tanks is critical

[*] Cryogenic Fluid Systems Engineer, Propulsion Division, NASA Glenn Research Center
[†] Research Professor, Aerospace and Mechanical Engineering, Case Western Reserve University
[‡‡] Research Professor, Aerospace and Mechanical Engineering, Case Western Reserve University
[§§] Mechanical Engineer, HX5
[**] Mechanical Engineer, HX5

for the effectiveness of guidance, navigation, and control systems. This is especially important to ensure stability and efficiency in space missions.

When cryogenic propellant tanks are pressurized, the gas condenses on the liquid surface, warming it up and releases heat due to phase change. If the tank is disturbed and sloshes, it can lead to more condensation and a rise in the propellant's temperature. This increase in temperature might result in a higher pressure in the tank, whether it's for storage in an on-orbit propellant depot or on a vehicle on an outbound mission to the Moon or Mars.

In orbit, as the propellant absorbs more heat, both its temperature and pressure can increase. To prevent exceeding the tank's pressure limits, the vapor may need to be vented. This venting, also known as boiloff, leads to a loss of propellant. NASA's tests have shown that sloshing can significantly increase the need for pressurant and the average temperature and pressure of the propellant.

In response, NASA is developing computational fluid dynamics models with advanced algorithms to better understand these complex processes, including the heat and mass transfer involved in condensation and evaporation. These models are tested against ground experiments to confirm their accuracy.

This work is part of NASA's long-term efforts to enhance the handling and management of cryogenic propellants, which are essential for the success of future space missions. By predicting in-space cryogenic operations which much integrate with management of guidance, navigation, and control systems used for these vehicles, the storage and transfer of cryogenic propellants can be optimized, contributing to the efficiency and success of space missions.

## COMPUTATIONAL FLUID DYNAMICS MODEL GOVERNING EQUATIONS

The computational fluid dynamics (CFD) approach described here effectively utilizes the Volume of Fluid (VOF) method to solve the Navier-Stokes equations. These equations, which include mass continuity, momentum, and energy, are crucial for understanding fluid flow and heat transfer in cryogenic propellant management. The details of the formulation can be found in Kassemi et al [2]. The fluid flow and heat transfer in the tank are described in terms of the continuity, momentum, and energy equations for both phases:

$$\frac{\partial \rho}{\partial t} + \nabla(\rho \mathbf{v}) = 0, \tag{1}$$

$$\frac{\partial}{\partial t}(\rho \mathbf{v}) + \nabla(\rho \mathbf{v}\mathbf{v}) = -\nabla p + \nabla\left[\mu_{eff}(\nabla \mathbf{v} + \nabla \mathbf{v}^T)\right] + \rho \mathbf{g} + \mathbf{F}_{vol}, \tag{2}$$

$$\frac{\partial}{\partial t}(\rho E) + \nabla\big(\mathbf{v}(\rho E + p)\big) = \nabla\big(k_{eff}\nabla T\big) + S_h. \tag{3}$$

In this case, the movement of the interface is captured diffusely by the model using the Volume of Fluid (VOF) method, as promulgated by Hirt and Nichols[3]. The interfacial energy, momentum, and mass balances are applied using source terms in the diffuse interfacial region. In the VOF method, a volume fraction is defined in each cell such that the volume fractions of all the phases sum to unity. In each cell, the change in the interface can be tracked by solving a continuity equation for the volume fraction of the qth phase:

$$\frac{1}{\rho_q}\left[\frac{\partial}{\partial t}(\alpha_q \rho_q) + \nabla \cdot (\alpha_q \rho_q \mathbf{v}_q) = S_{\alpha_q}\right], \tag{4}$$

where the volume fraction for the primary phase is determined from:

$$\sum_{q=1}^{n} \alpha_q = 1. \tag{5}$$

In the VOF method, the field variables and properties are defined in terms of the volume fraction, which for a general system can be written as:

$$\rho = \sum_{q=1}^{n} \alpha_q \rho_q, \qquad \mu_{eff} = \sum_{q=1}^{n} \alpha_q \mu_{eff_q}, \qquad k_{eff} = \sum_{q=1}^{n} \alpha_q k_{eff_q}. \tag{6}$$

In this fashion, the continuity, momentum, and energy equations, as described by Eq. (1) – (3), can be solved throughout the domain for the temperatures and velocities in the two phases. In the VOF model, the energy (E) and temperature (T) are treated as mass-averaged variables:

$$E = \frac{\sum_{q=1}^{n} \alpha_q \rho_q E_q}{\sum_{q=1}^{n} \alpha_q \rho_q}, \tag{7}$$

where $E_q$ is based on the specific heat of the qth phase and the shared temperature.

Evaporation and condensation at the interface are modeled as a source term in the continuity equation for the volume fraction (Eq. 4), i.e.:

$$S_{\alpha_q} = \dot{\mathbf{m}}_i \cdot \mathbf{A}_i \,, \tag{8}$$

where $\mathbf{A}_i$ is an interfacial area density vector, and $\dot{\mathbf{m}}$ is a mass flux vector, which for near equilibrium conditions can be determined based on the Schrage equation[4]:

$$|\dot{\mathbf{m}}| = \left(\frac{2\sigma}{2-\sigma}\right)\left(\frac{M}{2\pi R}\right)^{1/2}\left(\frac{P_i}{T_i^{1/2}} - \frac{P_v}{T_v^{1/2}}\right). \tag{9}$$

Here σ is the accommodation coefficient; M is the molar mass of the fluid; R is the universal gas constant; P*i* and $P_v$ are, respectively, the interfacial and vapor pressures (it is assumed that $P_i \cong P_{sat}$); T*i* and $T_v$ are, respectively, the interfacial and vapor temperatures (it is assumed that $T_i = T_v \cong T_{sat}$ at the interface). The range of accommodation coefficients used in these studies, between 0.001 and 0.01, is crucial, as this coefficient significantly influences the predictions, particularly the rate and amount of condensation. It's important to perform sensitivity studies on this coefficient, ensuring that the results are independent of variations in its value. Choosing an accommodation coefficient that is too low could underrepresent the phase change effects, such as condensation.

Additionally, the paper discusses the exploration of various turbulence models, including laminar flow, Reynolds Averaged Navier-Stokes (RANS) models like the k-omega SST model by Menter, and tests involving Large Eddy Simulation (LES) turbulence modeling. The interaction of turbulence with the VOF framework, particularly at the liquid-vapor interface, is important to consider. In VOF models' continuity of turbulence energy is assumed across the interface. But in reality, due to surface tension forces, turbulence can be considerably dampened by the interface. Since currently the VOF models do not consider dampening of turbulence at the interface, they predict very large effective turbulent conductivities at the phase front. These turbulent conductivi-

ties can be several orders of magnitude larger than the molecular conductivity that, due to turbulence dampening, may be the relevant conductivity that determines heat transfer at the interface. This leads to an augmented heat transfer rate across the interface that consequently causes an overprediction of the condensation rate. This discrepancy also results in a prediction of higher additional pressurant requirements, deviating from experimental measurements and observations.

## VALIDATION TESTS

NASA and its partners have used several cryogenic propellant tests to validate and refine their computational fluid dynamics (CFD) models. These tests, spanning from the development of the Saturn vehicles in the 1960s to more recent efforts, focus on understanding the behavior of liquid hydrogen and other cryogenic materials.

Key collaborations with international agencies like JAXA (Japan Aerospace Exploration Agency) and CNES (French National Centre for Space Studies) have provided valuable data and insights. These partnerships have been crucial in tackling the complex behaviors of cryogenic propellants.

The tests covered below include a range of scenarios:

- Liquid methane propellant pressurization and expulsion tests, both with and without sloshing effects.
- Liquid hydrogen autogenous pressurization and sloshing tests.
- Liquid nitrogen slosh experiments performed by JAXA and the University of Tokyo in 1g.
- Liquid nitrogen sloshing experiments performed by CNES in 1-g.

These tests and the associated CFD model validations have played a significant role in enhancing and confirming the accuracy of the predictive CFD models. They provide insights into how different cryogenic propellants behave under various conditions, contributing to a better understanding of cryogenic propellant management in space missions.

### Liquid Methane Propellant Expulsion and Pressurization with and without Sloshing (Ground)

In the 1960s, NASA conducted a series of cryogenic propellant expulsion tests using liquid methane, as documented in the Dewitt report[1]. These tests took place within the Ksite facility, a sizable vacuum facility, and involved various pressurants, including autogenous (methane), helium, hydrogen, and nitrogen. Figure 1 provides a visual representation of the 5 ft diameter test tank situated outside the Ksite Test Facility.


**Figure 1. 5 ft Diameter Tank Outside of Ksite Test Facility**

For both static and sloshing expulsion tests, the tank was initially filled to a 95% liquid methane level. Subsequently, it was pressurized to 3.4 bar using the appropriate pressurant. This pressure was maintained for an additional 24 seconds before initiating the liquid expulsion phase, ultimately reducing the liquid to a target fill level of 5%.

In 2023, Computational Fluid Dynamics (CFD) models were developed to simulate the expulsion tests, examining scenarios both with and without induced sloshing. The exhaustive 107-page test report was reviewed for candidate CFD validation tests. A select subset of these tests provided comprehensive data on pressurant characteristics, liquid outlet temperature, and liquid/vapor wall temperatures, serving as the foundation for the modeling validation efforts.

**Run 8-Static Expulsion Test**

Case 8 was chosen for modeling, employing a 226K autogenous pressurant gas to expel roughly 90% of the liquid within a 231-second timeframe. The simulation of the static expulsion test was performed using ANSYS FLUENT based on a 2D axisymmetric setup[5]. A full conjugate heat transfer analysis for the tank wall enabling heat transfer between the liquid/vapor and the tank wall. Simulations were performed to examine three different flow regimes: laminar, turbulent, and turbulent with damping at the liquid/vapor interface.

To maintain the tank pressure in line with the experimental controller's settings during the liquid drain phase, a controller was implemented within FLUENT. This controller dynamically adjusted the pressurant flow rate to match the target pressure recorded during the drain phase of the experiment .

Figure 2 shows the predicted liquid and vapor temperature during the static drain.

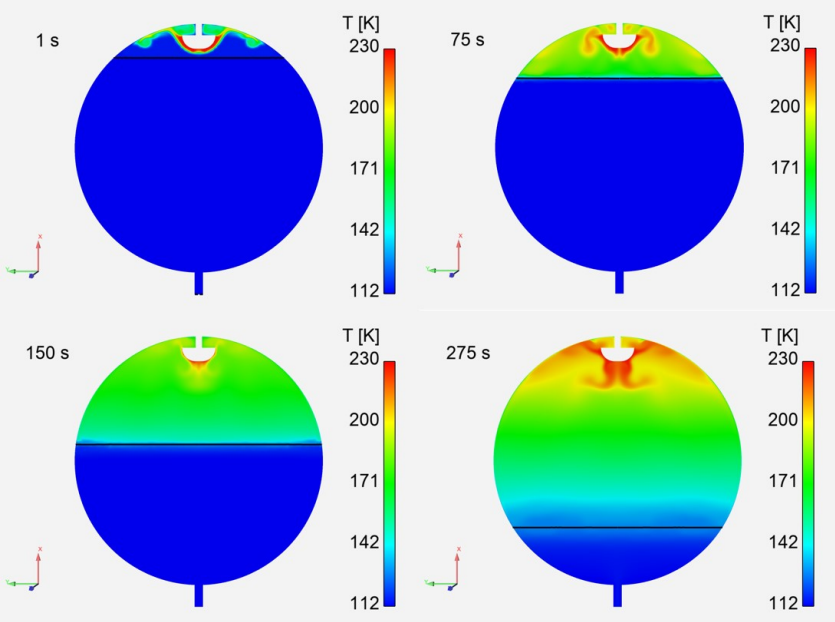


**Figure 2. Fluent Predicted Temperatures During Static Drain (Turbulent with damping).**

A comparison was made between the predicted pressurant mass required for expulsion and the experimental data, in addition to assessing the agreement between the tank wall temperatures and the liquid/vapor temperatures at the conclusion of the expulsion phase.

Furthermore, simulations were executed with three laminar and turbulent models of turbulence (k-omega, k-omega with damping at the liquid/vapor interface), and Figure 3 presents a comparison of the predicted pressurant mass versus the experimental pressurant mass for these models.

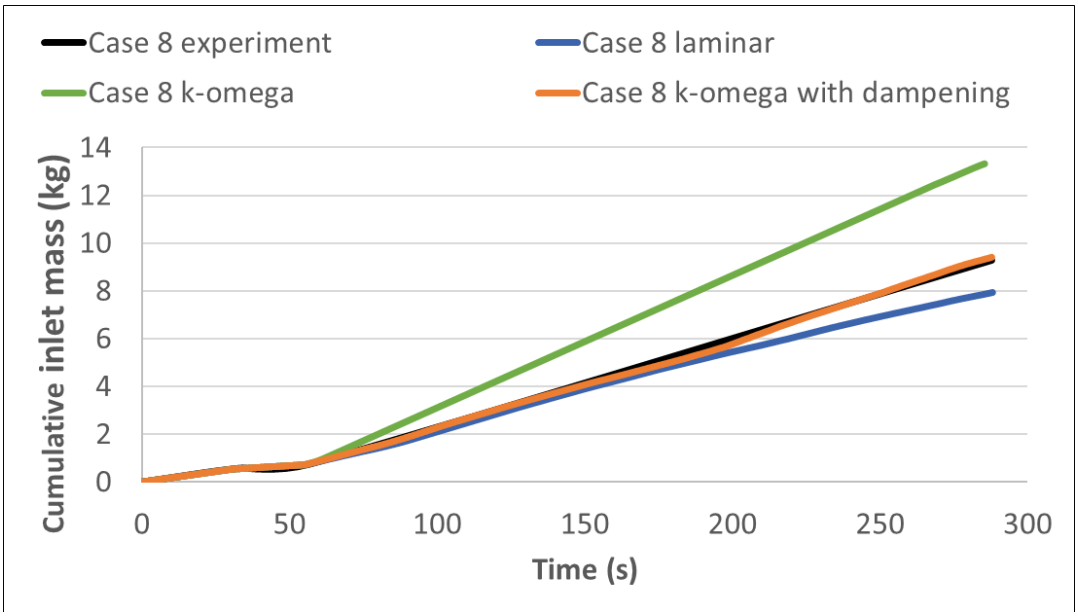


**Figure 3. Predicted Pressurant Mass for Laminar and Turbulence compared to the Experimentally Measured Pressurant Mass.**

The laminar model exhibited an underestimation of the required pressurant mass by approximately 10%. Conversely, the turbulence model without damping overestimated the pressurant mass by 45%. This overestimation in the turbulence model can be attributed to an enhanced effective thermal conductivity in the liquid, surpassing the molecular thermal conductivity seen in the laminar case with a value of 0.18 W/m-K. An illustration of the thermal conductivity of the liquid at 271 seconds into the drain is shown below (Figure 4a, 4b), illustrating that the effective turbulent thermal conductivity is nearly 1000 times greater than the laminar thermal conductivity.

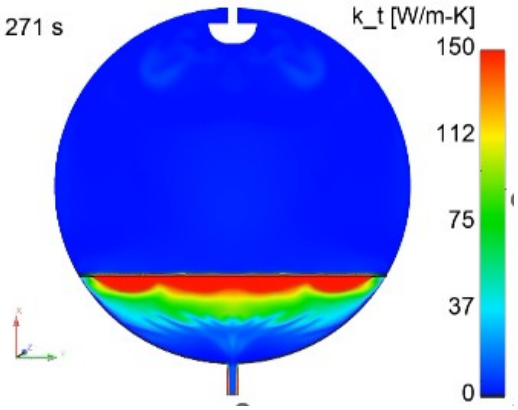


**Figure 4a. Effective Thermal Conductivity for Turbulent Case without Damping**

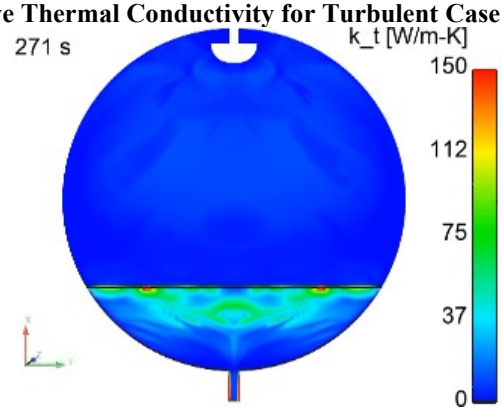


**Figure 4b. Effective Thermal Conductivity for Turbulent Case with Damping**

Upon enabling turbulence damping at the interface, the turbulence observed in the ullage region due to pressurant injection was significantly reduced within the liquid, resulting in a closer alignment between predicted and experimental pressurant behavior. The predicted pressurant closely matched the experimentally measured pressurant, differing by only a few percentage points (Figure 5). Figure 6 and 7 visually demonstrates the improved agreement between predicted and experimental ullage and wall temperatures at the conclusion of the drain.

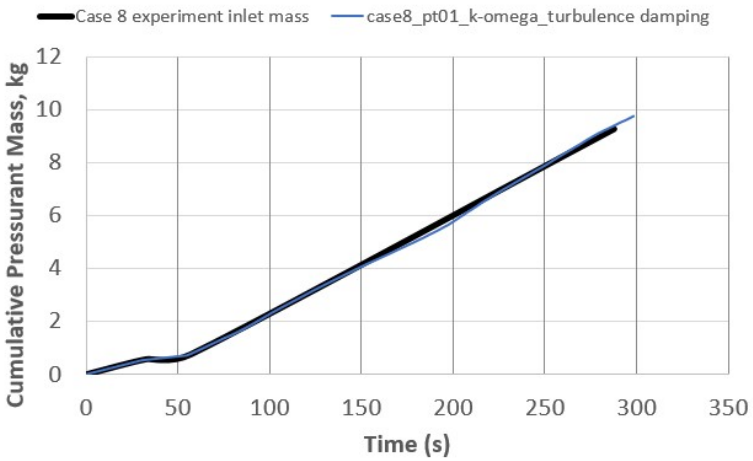


**Figure 5. Predicted Pressurant Mass for Turbulence with Interfacial Turbulence Damping compared to the Experimentally Measured Pressurant Mass.**

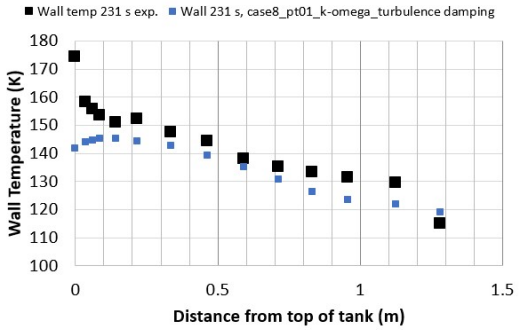


**Figure 6. Predicted vs Exp Final Wall Temperature**

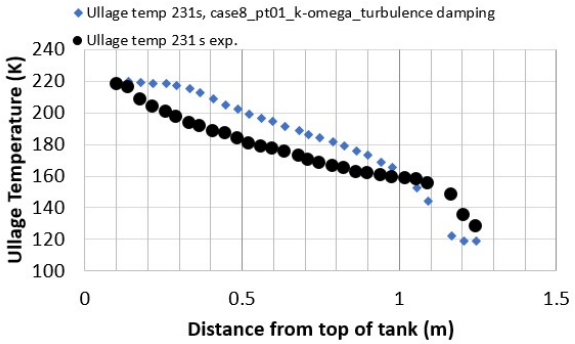


**Figure 7. Predicted vs Exp Final Ullage Temperature**

**Run 88- Expulsion Test with Sloshing**

An expulsion test with sloshing was also selected based on available data, including the measured experimental pressurant mass flow rates and the liquid outlet temperatures. During this test, the tank was subjected to controlled motion at a frequency of 0.716 Hz and an amplitude of 0.510 cm during the liquid expulsion phase. The autogenous pressurant temperature averaged 222 K throughout the expulsion process.

The test was simulated using ANSYS FLUENT with an approach similar as in the previous cases. Similar to the static drain case, wa full conjugate heat transfer analysis for the tank wall was performed. However, due to the 3D dynamic sloshing behavior of the liquid inside the tank, a 3-dimensional CFD model was devised to accurately capture the induced sloshing phenomena.

The CFD simulation encompassed the entire test sequence, including the pressurization phase, hold period, and propellant drain phase, during which the tank underwent controlled motion at the previously mentioned frequency and amplitude. Figure 8 illustrates the initial conditions within the tank at the onset of the propellant drain.

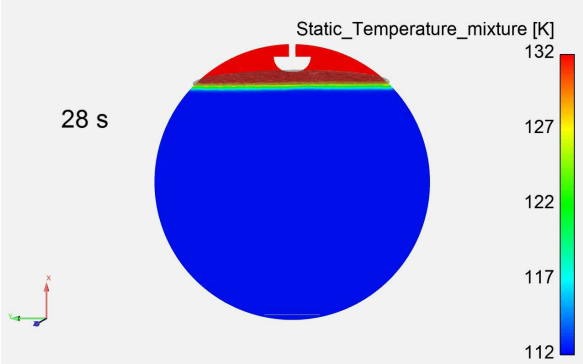


**Figure 8. Initial Propellant Temperatures During Drain (Case 88)**

Similar to the static drain case (Run 8), a pressurant controller was integrated into the model to maintain a constant pressure of 3.4 bar, aligning with the experimental conditions. Multiple simulations were conducted for this case, encompassing laminar and turbulent flow models with liquid/vapor interface damping.

The stability of propellant sloshing was examined previously by investigating various sloshing frequencies and amplitudes (Stofan/Amrstead and Sumner) in spherical tanks [6, 7]. Figure 9, presented below, illustrates the development of sloshing stability regions [8]. These regions are determined based on the ratio of the slosh frequency to the tank's natural frequency and the amplitude of sloshing. This determination helps distinguish between stable and unstable conditions, encompassing both planar and non-planar waves.

It has been observed that sloshing within stable regions results in minimal ullage collapse, whereas sloshing within the unstable regions, as demonstrated experimentally, leads to elevated pressure collapses. This phenomenon can be attributed to the heightened fluid motion generated during these operations, which can induce the circulation of subcooled cryogenic propellant near the liquid-vapor interface. This circulation results in increased condensation and a subsequent pressure drop.

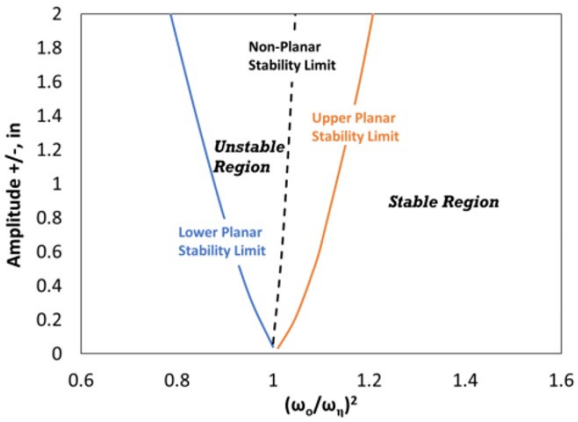


**Figure 9. Slosh Stability Map for 66% Fill Level in Spherical Tanks**

The Slosh Stability Map depicted in Figure 10 illustrates the stability of the liquid methane propellant as it drains from 95% to 5% fill level. This map is crucial in understanding how different fill levels impact the stability of the liquid within the tank. It is observed that when the propellant level drops to between 55% and 40%, there is a notable shift to instability.

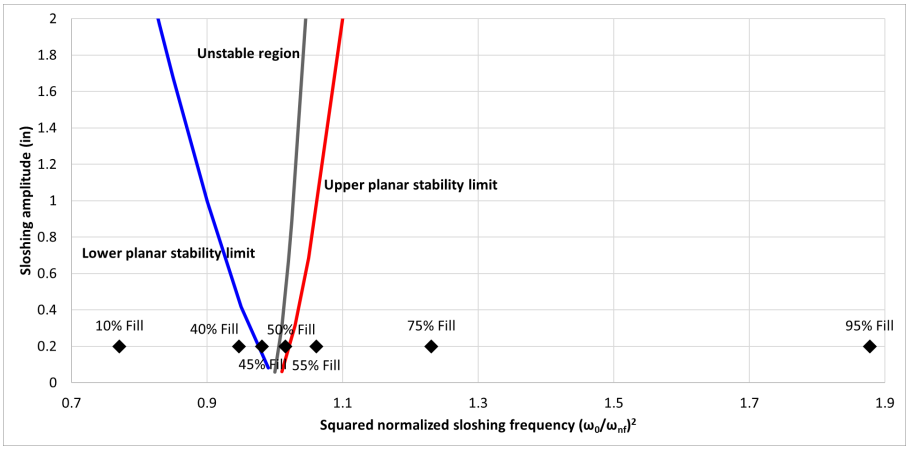


**Figure 10. Slosh Stability Map for Case 88 Liquid Expulsion (with annotated fill levels) for detailed insights.**

Complementing this, Figure 11 compares the predicted and experimental pressurant flow rates, shedding light on the discrepancies between the laminar and turbulent flow models. This figure corroborates the slosh stability findings, particularly highlighting the increased need for pressurant during the mid-phase of the expulsion – a phase where the liquid level is approximately at the midpoint of the tank.

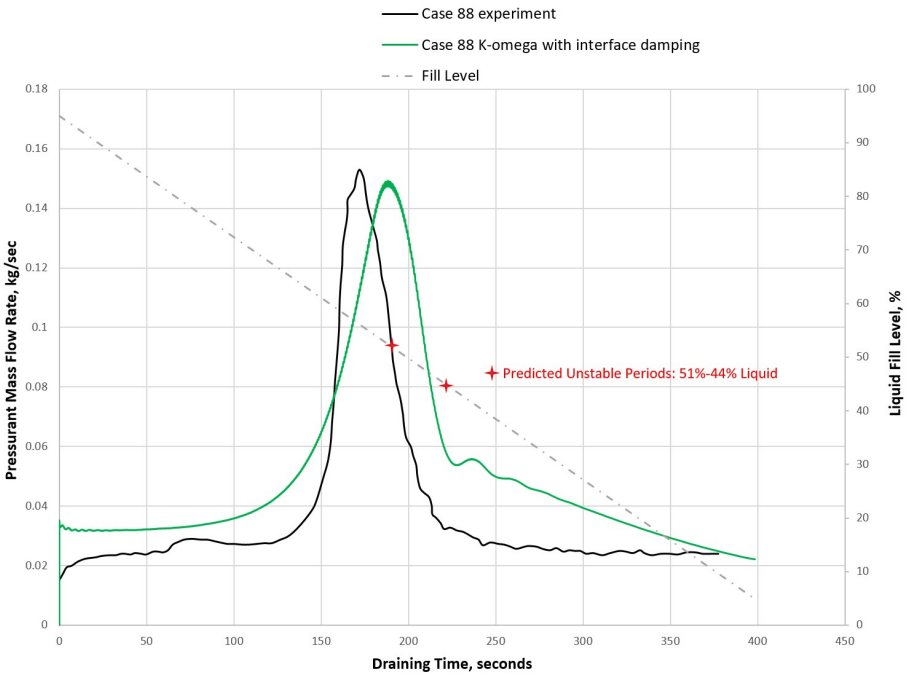


**Figure 11. Predicted Pressurant for Expulsion Test with Induced Sloshing (Case 88)]**

The rise in pressurization rate demand is primarily due to wave instability occurring around the mid-region of the draining process. Shown in Figures 12 a-d below are the predicted liquid temperatures and effective thermal conductivity during the drain. As shown in Figure 12a-d below, as the sloshing intensifies, these waves bring cooler liquid to the surface, increasing condensation and subsequently the need for a higher pressurant mass to maintain the target pressure of 3.4 bar throughout the expulsion phase. The models adeptly capture these intricate dynamics, offering essential insights into the pressurization needs during expulsion under conditions of induced sloshing.

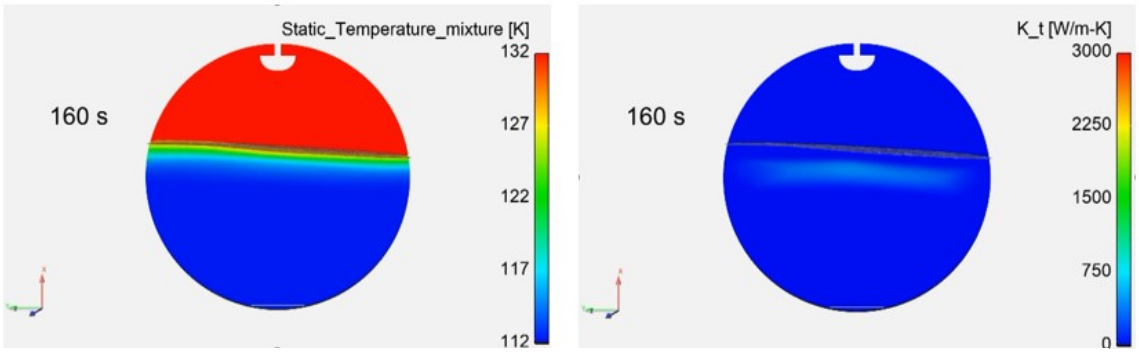


**Figure 12a.**

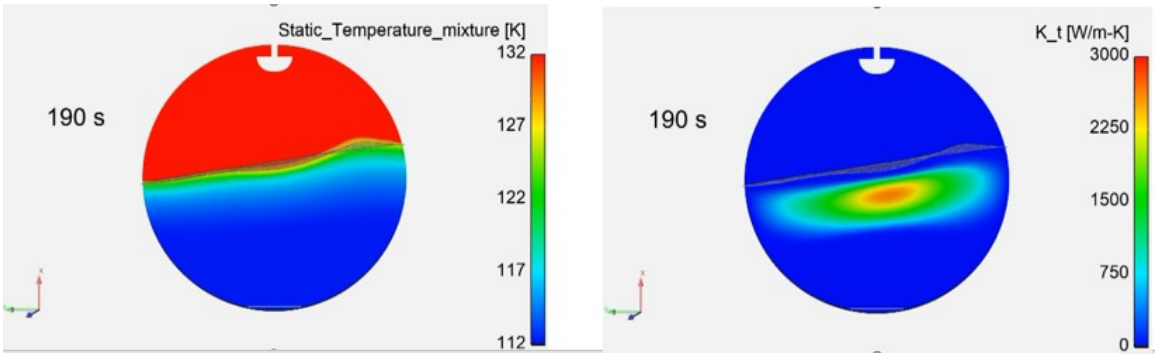


**Figure 12b.**

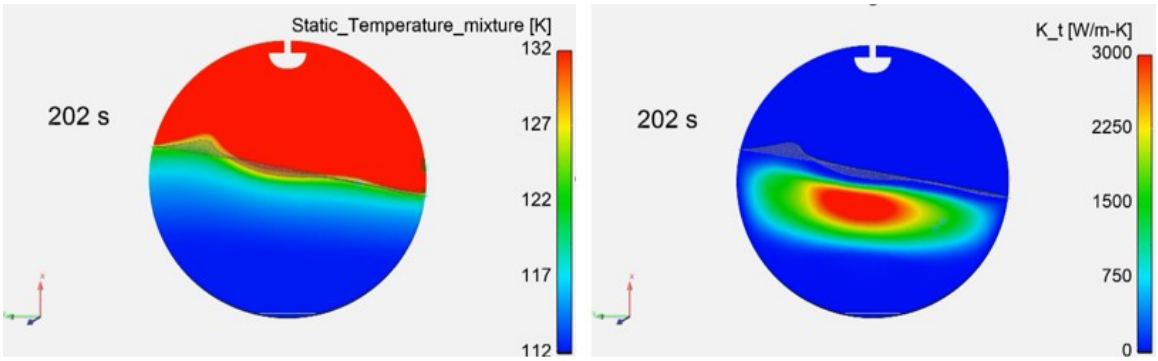


**Figure 12c.**

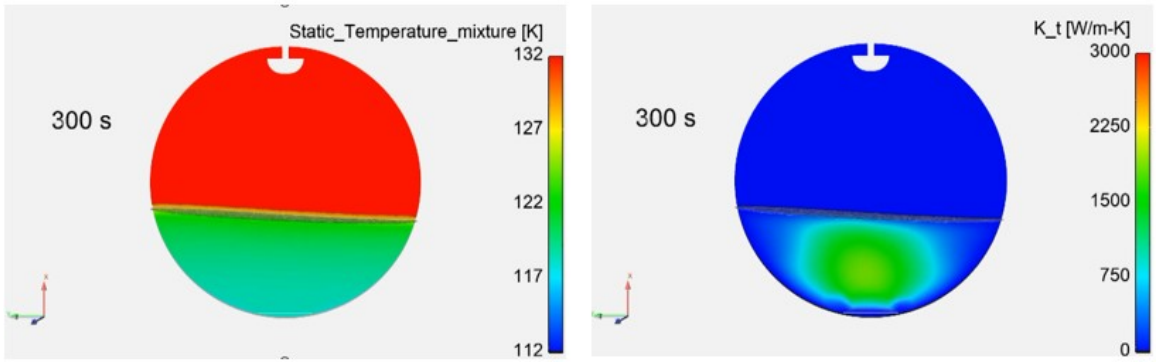


**Figure 12 a,b,c,d. Predicted Propellant Temperatures and Effective Thermal Conductivity During Drain (Case 88)**

**Liquid Hydrogen Autogenous Pressurization and Sloshing Tests (Ground)**

A couple decades later, NASA undertook another extensive research program spanning nearly a decade, focusing on the expulsion and slosh behavior of liquid hydrogen. These investigations encompassed tests conducted with both standard boiling point hydrogen and the "slush" hydrogen, which involves cooling a portion of the propellant below its freezing point. The principal motivation behind chilling the hydrogen was to capitalize on its latent heat of fusion, allowing it to absorb heat during various mission phases of in-space vehicles. The experiments employed the same 5-foot diameter aluminum tank, which had previously been utilized in the methane tank tests.

This work centers on the LH2 Ksite tests, specifically concentrating on pressurization and sloshing while excluding expulsion. The test details can be found in a 1994 paper authored by

Matt Moran [8]. To analyze these tests, an ANSYS FLUENT Computational Fluid Dynamics (CFD) model was employed to predict behavior during pressurization and sloshing, and these predictions were compared with experimental datasets[9].Two tests were chosen for modeling, one in the stable slosh region (Test 869) and one in the unstable slosh region (Test 870). Both tests encompassed pressurization, ramp or hold phases, and sloshing, and they were conducted with liquid fill levels of 67% and 64%, respectively.

Notably, Test 869 and Test 870 exhibited distinct sloshing characteristics. Test 869 featured sloshing with an amplitude and frequency of +/-0.5 inches and 0.95 Hz, respectively, while Test 870 displayed sloshing with an amplitude and frequency of +/- 1.5 inches and 0.75 Hz, respectively. The behavior of these cases can be visualized using the slosh stability map below in Figure 13. The map helps to illustrate their dynamics by considering the ratio of sloshing frequency to natural frequency and amplitude. Case 869 was identified within a stable region, while Case 870 resided in an unstable, non-planar region, suggesting the possible development of non-planar waves. These waves could potentially enhance heat and mass transfer between the warm ullage gases and the cold liquid.

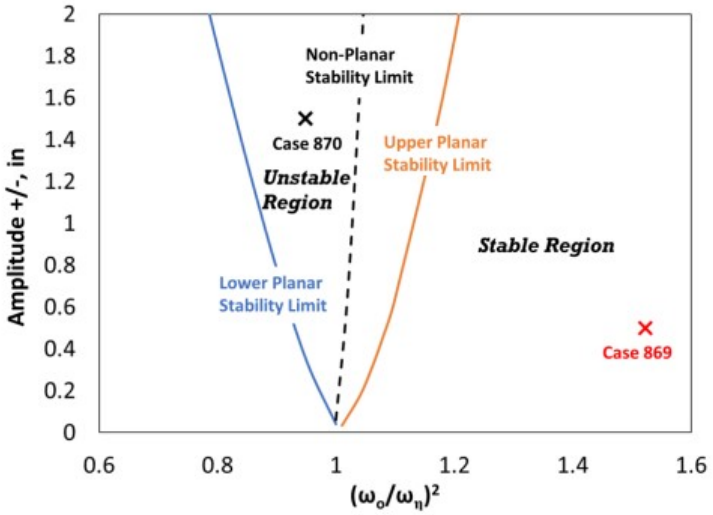


**Figure 13. Slosh stability map for cases 869 and 870**

Similar to the approach in the methane expulsion tests a full conjugate heat transfer analysis for the tank wall was performed to account for the heat exchange between the liquid/vapor and the tank walls.

Figure 14 presents a comparison between predicted tank pressures during pressurization, holding, and sloshing and the corresponding experimental data for both case 869 and 870. Notably, the CFD results closely align with the measured values, particularly during the pressure increase (ramp) and constant pressure (hold) phases of the tests. This alignment underscores the fidelity of the modeling and simulation techniques, providing valuable insights into the tank's behavior during these critical phases of the test.

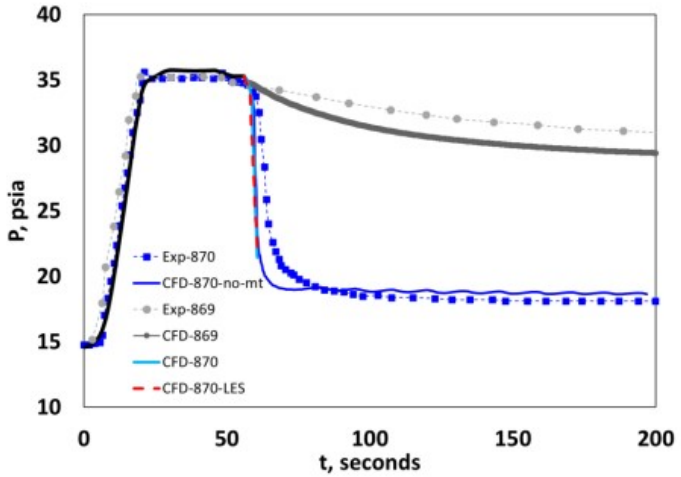


**Figure 14. Tank pressure during pressurization, hold, and sloshing after like-gas pressurization, Case 869 and 870: CFD vs. Experiment**

**JAXA Liquid Nitrogen Sloshing Experiments (Ground)**

As part of an international collaboration, NASA teamed up with JAXA to collaborate for mutual benefit utilizing experimental data on cryogenic nitrogen sloshing, supplementing this with Computational Fluid Dynamics (CFD) modeling. This setup featured a test cryostat, crafted from transparent polycarbonate and comprising a cylindrical section (0.105 meters in diameter) and a dome-shaped base, all insulated by a vacuum. Encased within a copper coolant jacket and vacuum chamber, the vessel enabled real-time observation of interface movements via a high-speed camera and facilitated monitoring of internal pressure and temperature changes using a pressure transducer and five thermometers. Additional details on the experiment's intricacies are found in Himeno's work [10].

The experiment's protocol involved first conditioning liquid nitrogen, followed by its pressurization with gaseous nitrogen. Sloshing was then induced by applying lateral acceleration to the tank.

To complement the physical experiment, the NASA team conducted a simulation using ANSYS FLUENT[11]. This mirrored prior modeling methods discussed in the paper, with a full conjugate heat transfer analysis for the tank wall. A 3D CFD model was essential for accurately capturing the fluid's dynamic sloshing behavior. Figure 15 below shows the predicted liquid movement compared the movement observed during the experiment.

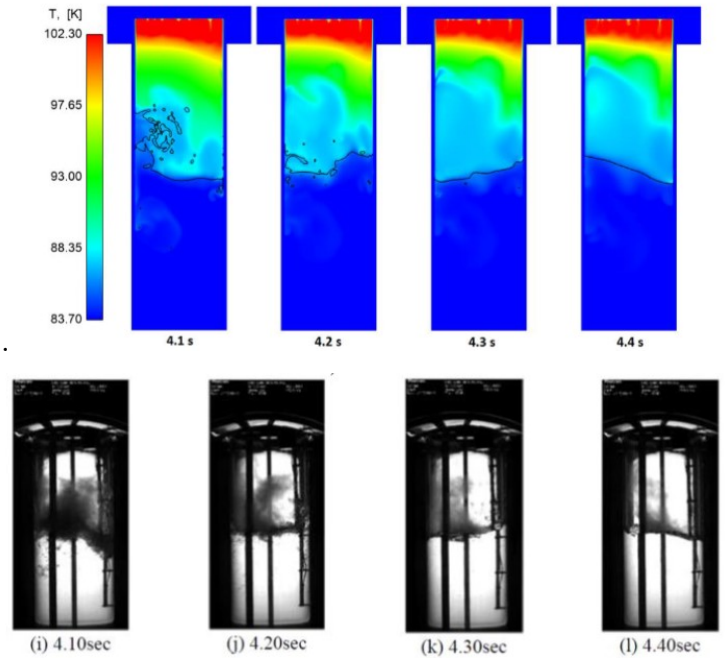


**Figure 15. Juxtaposes the predicted liquid movements from the CFD model against those observed in the actual experiment, showcasing a strong correlation in interface movement.**

Another crucial aspect of the study, depicted in Figure 16, involves comparing predicted and measured pressures collapses during the sloshing event. The graph reflects uncertainties in the tank's upper wall temperatures due to the lack of experimental data. So simulations were performed to examine predictions under two scenarios: 'cold wall' and 'matching wall'—the former using the colder measured initial liquid temperature for the entire wall and the latter aligning the wall temperature with the measured initial fluid temperature in the tank at the same height. Notably, both models accurately predict the steep decrease in pressure, aligning well with the experimental data.

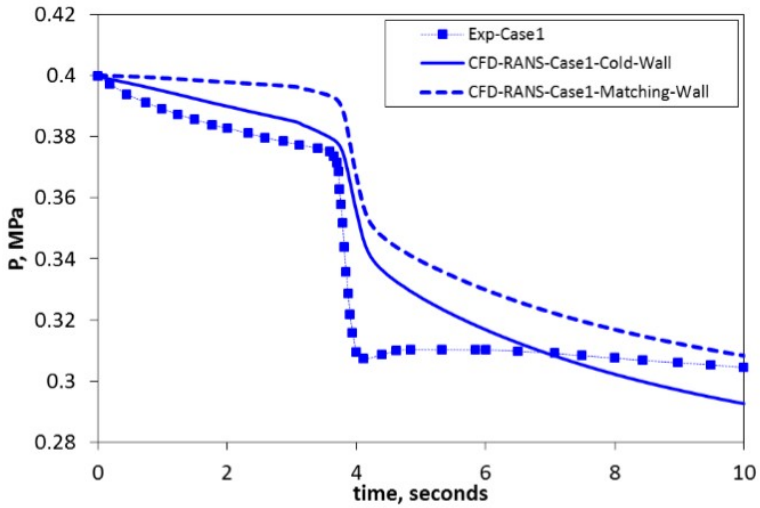


**Figure 16. Predicted vs. Measured Pressure Evolution in the Tank During Sloshing - Case 1, examining the effect of 'cold' and 'matching' wall initial conditions.**

A similar analysis was performed using the Flow-3D Volume-Of-Fluid (VOF) CFD solver. Basic LN2 tank dimensions followed the drawings supplied by JAXA, with 110mm ID and 340mm height. Heat transfer and phase change was included in the simulation so the 4.5mm thick acrylic cylinder and 30mm high "top hat" at the top of the cylinder were included. Total computational space encompassed the tank itself, adjoining tank walls, and some surrounding solid space, for overall dimension of 80mm x 80mm x 400mm. Sensitivity was done on the cell dimensions and it was found that 4mm cells were sufficiently small, such that the total model size was a relatively small 160,000 cells; simulations were able to be carried out on a laptop computer in about one hour. A range of accommodation coefficients was considered and consistent results were obtained using a coefficient of 1E-3.

Ullage collapse tests were simulated. In the tests, the tank was subjected to an approximate 1.2g back and forth acceleration over 0.435 seconds; the Non-Inertial Reference Frame feature in Flow-3D was used to capture this applied acceleration. The tank wall itself was chilled in to 77K at the start of the test. Four different initial configurations were considered, with warm layers of 5, 30, 80, and 130mm (Figure 17). Assumed temperatures of the bulk, stratified, and vapor temperatures were 83.7K, 91.3K, and 96.0K respectively; no gradients within those regions were assumed for this study. The test apparatus contained 5 thermocouple probes, indicated by red boxes in the figure below, and designated T1 (top) through T5 (bottom).

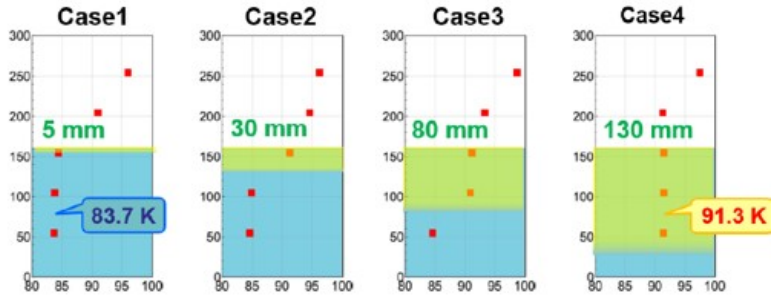


**Figure 17. Initial Temperature Liquid Temperatures**

Primary outputs of this study were ullage pressure and fluid temperature. As expected, the pressure collapse for the 5mm stratified layer case was much larger than for the others because more cold liquid interacted with the ullage. A side-by-side comparison in Figure 18 below (test data on left, Flow-3D on right) produced good results:

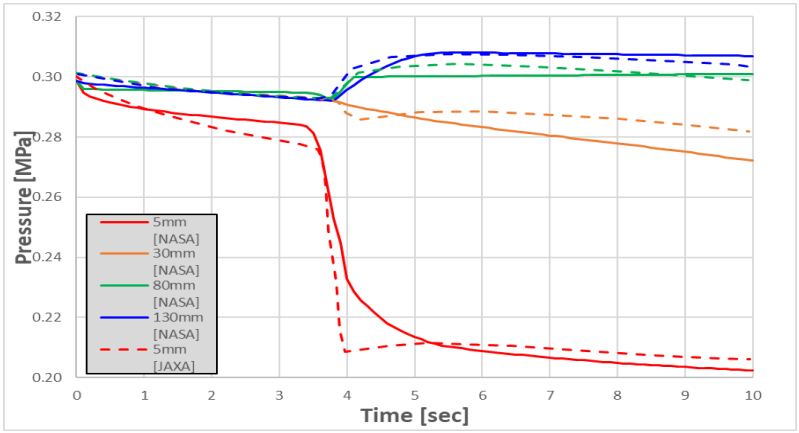


**Figure 18. Comparison of Experimental Pressure Signatures versus CFD- Predicted (Flow-3D) Pressure Signatures Across Various Stratification Levels**

Temperature within the liquid was compared to test data as well in Figure 19. This data is a comparison for the 5mm stratified layer case. Note that the ullage is cooled almost to saturation temperature, whereas there was insufficient mixing to warm up the lower layers of the tank sufficiently.

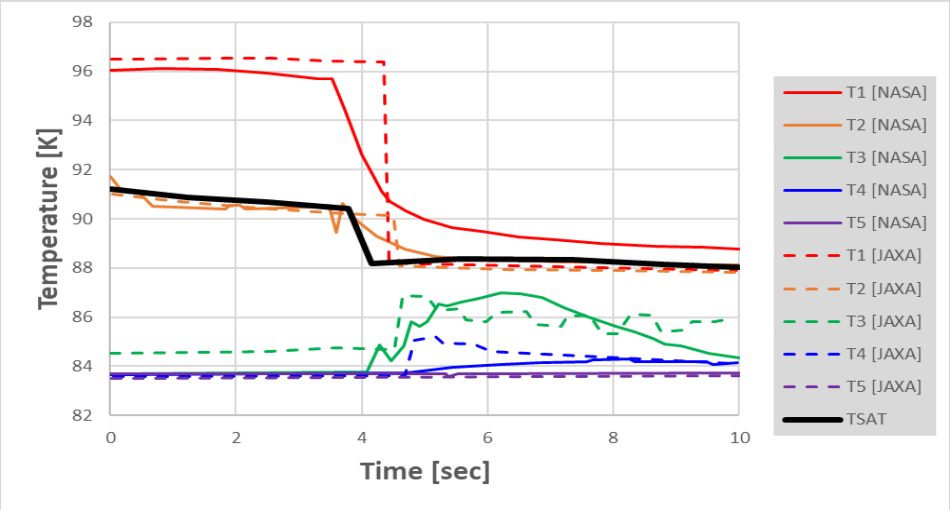


**Figure 19. Comparison of Experimental Temperature Signatures versus CFD- Predicted (Flow-3D) Temperature Signatures.**

### CNES Liquid Nitrogen Sloshing Experiments (Ground)

In this collaborative project between NASA and CNES, NASA simulated a CNES experiment on cryogenic sloshing[12]. The experiments were initiated with the tank containing liquid nitrogen self-pressurized and thermally stratified, adhering to an initial temperature field derived from the CNES's experimental data. This thermal stratification was predominantly confined to the tank's ullage region. The tank underwent sinusoidal lateral shaking at a frequency of 2.1 Hz and a displacement of 3 mm, closely matching the natural frequency of the partially filled tank system.

To supplement the physical experiments, simulations were conducted by the NASA team using ANSYS FLUENT [13]. These simulations followed previously discussed methodologies in the paper, the authors did not include the conjugate heat transfer. A 3D CFD model was implemented to accurately depicting the liquid's dynamic sloshing behavior within the tank.

Comparisons between the predictions and CNES's experimental data are presented in Figure 20. During the initial phase, the experimental data showed a more gradual pressure decrease than the modeling results. Despite incorporating a time constant (as per Eq. 7) based on experimental data into the model, the simulations failed to replicate this slower experimental depressurization. Two modeling scenarios are discussed for comparison. In the first scenario, where the fluid flow in both the liquid and ullage regions is modeled as laminar, the depressurization appears slower compared to the experimental data. Conversely, when turbulence is modeled using a κ-ω SST model, the resulting thermal mixing significantly impacts the outcome, causing a more substantial pressure drop. Notably, the turbulent model's pressure closely aligns with the experimental data, particularly after the 20-second mark.

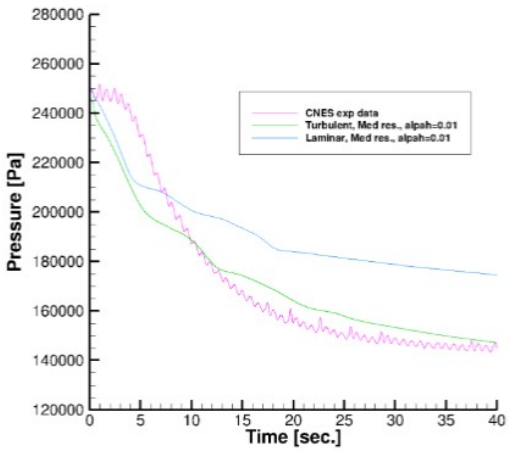


**Figure 20. This figure illustrates the predicted pressure during sloshing versus the experimentally measured pressure, comparing turbulent and laminar predictions.**

## CONCLUSION

In conclusion, NASA's advancement in computational fluid dynamics, integrated with interfacial heat mass transfer algorithms, is pivotal for accurately modeling phase change processes in cryogenic propellant tanks. These processes are essential for understanding the cryogenic propellant's behavior, particularly how superheated pressurant gas can condense into the subcooled liquid. This phenomenon presents a significant challenge in storing and transferring cryogenic propellants, necessitating additional onboard pressurant and affecting the temperature and pressure of the liquid propellant transferred. These models have been validated through several cryogenic slosh tests, with and without expulsion, showing strong agreement with experimental data.

However, further research is needed to fully understand the impact of non-condensable gases like helium on these phase change processes. Current algorithms for predicting phase changes in the presence of non-condensable are still in development. Fortunately, once these algorithms have been developed, NASA has conducted relevant tests with gaseous helium that can be used to anchor and prove their capability at predicting with a high degree of accuracy.

## REFERENCES


[1] Dewitt, R., Mcintire, T., “Pressurant requirements for discharge of liquid methane from a 1.52-meter-(5-ft-) diameter spherical tank under both static and slosh conditions”, NASA TN-D-7638, May 1974

[2]M. Kassemi, O. Kartuzova, S. Hylton, Validation of Two-Phase CFD Models for Propellant Tank Self-Pressurization: Crossing Fluid Types, Scales, and Gravity Levels, Cryogenics Vol. 89 pp. 1–15, Jan 2018.

[3] C.W. Hirt and B.D. Nichols, “Volume of fluid (VOF) method for the dynamics of free boundaries”, Journal of Computational Physics 39 (1): 201-225. 1981

[4] R.W. Schrage, A theoretical study of interphase mass transfer, Columbia University Press, New York, 1953.

[5] Baker, M., Hauser, D., Kartuzova, O., “CFD Modeling of a Cryogenic Methane Drain Test with and without Induced Sloshing” Space Cryogenics Workshop, July 2023, Kona, HI

[6] Stofan, A.J., and Armstead, A.L., "Analytical and Experimental Investigation of Forces and Frequencies Resulting from Liquid Sloshing in a Spherical Tank", NASA TN D-1281, July, 1962.

[7] Sumner, LE., Experimental Investigation of Stability Boundaries for Planar and Nonplanar Sloshing in Spherical Tanks", NASA TN D-321O, January, 1966.

[8] Moran, M.E. et-al., “Experimental Results of Hydrogen Slosh in a 62 Cubic Foot (1750 Liter) Tank”, NASA TM 106625, 1994

[9] Kartuzova, O., Kassemi, M., et-al, “Validation of a Two Phase CFD model for Predicting Tank Pressurization and Pressure Collapse in the Ground Based K-Site Hydrogen Slosh Experiment” AIAA SciTech Conference, January 2024, Orlando, FL, AIAA

[10] T. Himeno, et al., “Investigation on Phase Change and Pressure Drop Enhanced by Violent Sloshing of Cryogenic Fluid”, AIAA Propulsion and Energy Forum, July 2018, Cincinnati, OH, AIAA 2018-475

[11] Kartuzova, O, Kassemi, M, etal., “CFD Modeling of Phase Change and Pressure Drop during Violent Sloshing of Cryogenic Fluid in a Small-Scale Tank” AIAA Propulsion Conference, July 2020, Virtual, AIAA 2020-3794

[12] Lacapere, J., Vielle, B., and Legrand, B. (2009) “Experimental and Numerical Results of Sloshing with Cryogenic Fluids.” Progress in Propulsion Physics, vol. 1, pp. 267-278

[13] Agui, J.H., and Moder, J.P., “Modeling of Non-isothermal Cryogenic Fluid Sloshing” AIAA Propulsion Conference, July 2015, Orlando, FL, AIAA 2015-4072